

Trifluoromethyl-Substituted Iridium(III) Complexes: From Photophysics to Photooxidation of a Biological Target

Robin Bevernaegie,[†] Lionel Marcéls,^{†,||} Baptiste Laramée-Milette,[‡] Julien De Winter,[§] Koen Robeyns,[†] Pascal Gerbaux,[§] Garry S. Hanan,^{‡,||} and Benjamin Elias^{*,†}

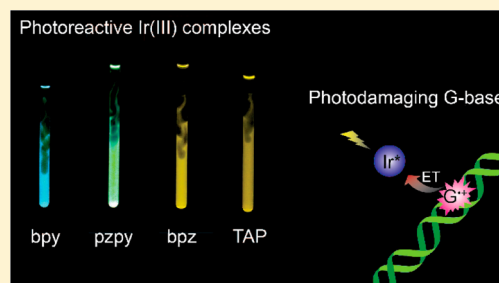
[†]Université catholique de Louvain (UCL), Institut de la Matière Condensée et des Nanosciences (IMCN), Place Louis Pasteur, 1 box L4.01.02, B-1348 Louvain-la-Neuve, Belgium

[‡]Département de Chimie, Université de Montréal, Pavillon J.-A. Bombardier, 5155 Chemin de la Rampe, Montréal, Québec H3T 2B1, Canada

[§]Organic Synthesis and Mass Spectrometry Laboratory, University of Mons – UMONS, 23 Place du Parc, B-7000 Mons, Belgium

Supporting Information

ABSTRACT: Photodynamic therapeutic agents are of key interest in developing new strategies to develop more specific and efficient anticancer treatments. In comparison to classical chemotherapeutic agents, the activity of photodynamic therapeutic compounds can be finely controlled thanks to the light triggering of their photoreactivity. The development of type I photosensitizing agents, which do not rely on the production of ROS, is highly desirable. In this context, we developed new iridium(III) complexes which are able to photoreact with biomolecules; namely, our Ir(III) complexes can oxidize guanine residues under visible light irradiation. We report the synthesis and extensive photophysical characterization of four new Ir(III) complexes, $[\text{Ir}(\text{ppyCF}_3)_2(\text{N}^{\wedge}\text{N})]^+$ [$\text{ppyCF}_3 = 2-(3,5\text{-bis}-(\text{trifluoromethyl})\text{phenyl})\text{pyridine}$ and $\text{N}^{\wedge}\text{N} = 2,2'\text{-dipyridyl (bpy)}$; $2\text{-}(\text{pyridin-2-yl})\text{pyrazine (pzpy)}$; $2,2'\text{-bipyrazine (bpz)}$; $1,4,5,8\text{-tetraazaphenanthrene (TAP)}$]. In addition to an extensive experimental and theoretical study of the photophysics of these complexes, we characterize their photoreactivity toward model redox-active targets and the relevant biological target, the guanine base. We demonstrate that photoinduced electron transfer takes place between the excited Ir(III) complex and guanine which leads to the formation of stable photoproducts, indicating that the targeted guanine is irreversibly damaged. These results pave the way to the elaboration of new type I photosensitizers for targeting cancerous cells.



INTRODUCTION

For many years, ruthenium(II) polypyridyl complexes have attracted much interest, thanks to their photophysical properties. They have been exploited not only in various fields such as photocatalysis,^{1–5} molecular antennas,^{6–8} and solar energy conversion^{9–11} but also in biological applications.^{12–14} In this area, the turning point was the discovery of the light-switch effect of $[\text{Ru}(\text{bpy})_2\text{dppz}]^{2+}$ (bpy = 2,2'-bipyridine, dppz = dipyrido[3,2-:2',3'-]phenazine) in the presence of DNA; the luminescence of the complex, which is quenched in aqueous media, is recovered after intercalation of the dppz ligand inside the DNA backbone.¹⁵ Increasing research in the field of biomedical applications was then performed by modifying the core of the dppz ligand. Thereby, novel Ru(II) complexes were developed to recognize not only specific DNA topologies^{16–18} (e.g., duplex vs G-quadruplex) but also the presence of defects in the double strand^{19–21} (e.g., mismatches, abasic sites, ...). In all of these cases, the ability of the complex to probe these specific targets depends on the nature of the extended planar ligand chelated to the metal center. Other Ru(II) complexes were developed by changing bpy ancillary ligands to pyrazine-based ligands such as bpz^{22,23} (2,2'-bipyrazine), TAP²⁴ (1,4,5,8-

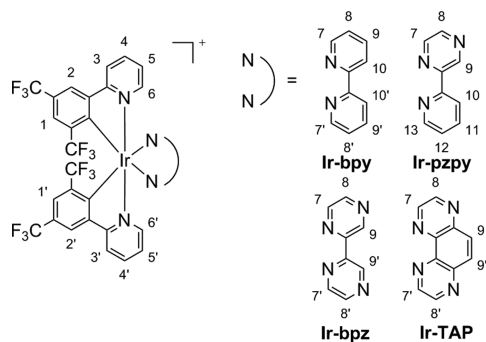
tetraazaphenanthrene), and HAT^{25,26} (1,4,5,8,9,12-hexaazatriphenylene). These modifications allow one to tune the photoreactivity of the resulting complexes, giving rise to highly photo-oxidizing compounds able to abstract, under irradiation, an electron from guanine residues of the DNA. This photoinduced electron transfer (PET) produces radical species (i.e., oxidized guanine residue along with the monoreduced complex) responsible for DNA cleavage²⁷ and/or the formation of adducts.²⁸ Such photoreactivity, termed type I (i.e., electron transfer), can be used to block replication and transcription of DNA.^{29–31} Therefore, these highly photo-oxidizing complexes constitute potential candidates in anticancer phototherapy when type II photoreactivity, i.e. production of ROS by energy transfer, is unsuitable (e.g., hypoxia tumor). Unfortunately, these photooxidant ruthenium-based drugs are unable to cross the membrane of living cells and to reach their biological target (i.e., nuclear or mitochondrial DNA), even if they are tethered to a cell-penetrating peptide, such as the TAT peptide.³²

Received: October 31, 2017

In this context, we were interested in replacing the Ru(II) metal center by Ir(III). Indeed, iridium(III) complexes have recently emerged as potential candidates in anticancer photo-therapy thanks to their exceptional photophysical properties, their good photostability, and their cell permeability.^{33–35} Moreover, their photoredox properties can be easily tuned by changing the C/N ratio in the first coordination sphere.³⁶ Nevertheless, there are only few examples of tris-bidentate complexes with a C/N ratio of 0/6 and consequently a high photo-oxidant power.^{37,38} Bis- and tris-cyclometalated compounds with C/N ratios of 2/4 and 3/3 not only are more common but also show a more photoreducing behavior due to the electron-donor character of the Ir–C bond.^{36,38} Therefore, it is still challenging to build new highly photo-oxidizing Ir(III) complexes.

In this work, we report the synthesis and characterization of four new bis-cyclometalated complexes obtained from the coordination of a fluorinated phenylpyridine ligand (ppyCF₃ = 2-(3,5-bis(trifluoromethyl)phenyl)pyridine) and four different diimine ligands (bpy = 2,2'-dipyridyl; pzpy = 2-(pyridin-2-yl)pyrazine; bpz = 2,2'-bipyrazine; TAP = 1,4,5,8-tetraazaphenanthrene). They are respectively termed hereafter **Ir-bpy**, **Ir-pzpy**, **Ir-bpz**, and **Ir-TAP** (Chart 1). The selection of such a

Chart 1. Structures of Ir-bpy, Ir-pzpy, Ir-bpz, and Ir-TAP



carbometalated ligand is explained by the presence of two electron-withdrawing groups on it to sufficiently deprive the Ir–C bond of electron density, consequently increasing the photooxidizing power of the target complexes. Photophysical properties of the four compounds were investigated from an experimental and theoretical approach, providing arguments in favor of mixed ligand centered (LC) and metal–ligand to ligand charge transfer (MLLCT) excited states. Their photo-reductant and photo-oxidant properties were assessed in the presence of a sacrificial electron donor and acceptor in organic solvent. Finally, we investigated their photoreactivity in the presence of guanine residue in aqueous buffer.

EXPERIMENTAL SECTION

All solvents and reagents for the synthesis were of reagent grade and were used without further purification. All solvents for the spectroscopic and electrochemical measurements were of spectroscopic grade. Water was purified with a Millipore Milli-Q system. ¹H NMR, ¹³C NMR, and ¹⁹F NMR experiments were performed in CD₃CN on a Bruker AC-300 Avance II (300 MHz) or Bruker AM-500 spectrometer (500 MHz) at 20 °C. The chemical shifts (given in ppm) were measured versus the residual peak of the solvent as an internal standard. High-resolution mass spectrometry (HRMS) was performed with a Q-Exactive orbitrap from ThermoFisher using reserpine as the internal standard. Samples were ionized by electrospray ionization (ESI), and the typical source conditions were as follows: capillary

temperature 320 °C, vaporizer temperature 320 °C, sheath gas flow rate 5 mL/min. Diffraction data were collected on a MAR345 image plate using monochromated (Xenocs Fox3D mirror) Mo K α radiation (Rotating anode, Rigaku UltraX 18S). All diffraction images were integrated by CrysAlisPRO,³⁹ and the implemented absorption correction was applied. The structures were solved by SHELXT⁴⁰ and refined by full-matrix least squares against |F²| using SHELXL-2014.⁴¹ All non-hydrogen atoms were refined anisotropically, and hydrogen atoms were placed on calculated positions with temperature factors fixed at 1.2 times the U_{eq} value of the parent atoms. HPLC traces were obtained for each complex on a Waters Alliance 2690 using an XBridge C18 column (50 × 4.6 mm, 2.5 μ m) as the stationary phase. The elutions were performed with a gradient starting from 90/10 water/acetonitrile (0.1% TFA) to 10/90 water/acetonitrile (0.1% TFA).

IrCl₃·xH₂O (PressChem), 2-bromopyridine (Acros), 2-chloropyridazine (Acros), 3,5-bis(trifluoromethyl)bromobenzene (Fluorochem), 2,2'-dipyridyl (bpy) (TCI), deoxyguanosine-5'-monophosphate disodium salt (dGMP) (Alfa Aesar), guanosine 5'-monophosphate disodium salt hydrate (GMP) (TCI), and ethylene glycol (Roth) were of reagent grade and were used without further purification. 2-(3,5-Bis(trifluoromethyl)phenyl)pyridine (ppyCF₃),⁴² 2-(pyridin-2-yl)pyrazine (pzpy),⁴³ 2,2'-bipyrazine (bpz),⁴⁴ 1,4,5,8-tetraazaphenanthrene (TAP),⁴⁵ and the cyclometalated Ir(III) chloro-bridged dimer [Ir(ppyCF₃)₂Cl]₂⁴² were synthesized according to the literature.

General Method for Complex Synthesis. The cyclometalated Ir(III) chloro-bridged dimer [Ir(ppyCF₃)₂Cl]₂ (40.4 mg, 0.025 mmol, 1 equiv) and the corresponding ligand L (0.055 mmol, 2.2 equiv) were suspended in 4 mL of ethylene glycol. The mixture was heated for 5 h at 150 °C under an argon atmosphere in the dark. After the mixture was cooled to room temperature, 10 mL of a saturated aqueous solution of NH₄PF₆ was added. Then, the precipitate was centrifuged and washed successively with water (three times), ethanol, and diethyl ether to finally give a yellow-orange powder after drying under vacuum.

Ir-bpy. [Ir(ppyCF₃)₂bpy]⁺PF₆[−] was obtained by using the synthetic procedure described above with 2,2'-dipyridyl as ligand L (8.6 mg, 0.055 mmol, 2.2 equiv), to give a pale yellow powder (35 mg, 65% yield). ¹H NMR (500 MHz, CD₃CN): δ 8.44 (H₁, H₁₁, H₁₀ and H_{10'}, m, 4H), 8.24 (H₃ and H_{3'}, d, J_{3(3')-4(4')} = 7.8 Hz, 2H), 8.15 (H₉ and H_{9'}, td, J_{8/10(8'/10')-9(9')} = 8 Hz and J_{7(7')-9(9')} = 1.4 Hz, 2H), 7.84 (H₄ and H_{4'}, td, J_{3/5(3'/5')-4(4')} = 7.8 Hz and J_{4(4')-6(6')} = 1.3 Hz, 2H), 7.78 (H₂, H_{2'}, H₇ and H_{7'}, m, 4H), 7.50 (H₈ and H_{8'}, m, 2H), 7.29 (H₆ and H_{6'}, d, J_{5(5')-6(6')} = 5.9 Hz, 2H), 6.96 (H₅ and H_{5'}, td, J_{5(5')-6(6')} = 5.9 Hz and J_{3(3')-5(5')} = 1.2 Hz, 2H). ¹⁹F NMR (282 MHz, CD₃CN): δ −59.76 (s), −62.97 (s), −72.94 (d, J_{F-31p} = 706.4 Hz). ¹³C NMR (75 MHz, CD₃CN): δ 166.40, 156.27, 151.94, 151.30, 150.74, 150.28, 141.80, 140.31, 137.31, 136.91, 130.38, 126.42, 124.92, 121.81. HRMS (ESI): *m/z* calculated for [C₃₆H₂₀N₄F₁₂¹⁹³Ir − PF₆]⁺ 929.11201; found 929.11095.

Ir-pzpy. [Ir(ppyCF₃)₂pzpy]⁺PF₆[−] was obtained by using the synthetic procedure described above with 2-(pyridin-2-yl)pyrazine as ligand L (8.6 mg, 0.055 mmol, 2.2 equiv), to give a yellow powder (32.2 mg, 60% yield). ¹H NMR (500 MHz, CD₃CN): δ 9.64 (H₉, d, J₈₋₉ = 1.2 Hz, 1H), 8.69 (H₇, d, J₇₋₈ = 3.1 Hz, 1H), 8.56 (H₁₀, d, J₁₀₋₁₁ = 8.1 Hz, 1H), 8.46 (H₁ and H_{1'}, s, 2H), 8.25 (H₃ and H_{3'}, m, 2H), 8.20 (H₁₁, dt, J_{10/12-11} = 8.0 Hz, J₁₁₋₁₃ = 1.5 Hz, 1H), 7.89–7.84 (H₄ and H_{4'}, m, 2H), 7.80 (H₂, H_{2'} and H₁₃, m, 3H), 7.74 (H₈, dd, J₇₋₈ = 3.1 Hz, J₈₋₉ = 1.2 Hz, 1H), 7.58 (H₁₂, ddd, J₁₁₋₁₂ = 7.7 Hz, J₁₂₋₁₃ = 5.6 Hz, J₁₀₋₁₂ = 1.2 Hz, 1H), 7.32 (H_{6'}, d, J₅₋₆ = 5.9 Hz, 1H), 7.27 (H₆, d, J_{5'-6'} = 6.0 Hz, 1H), 7.01–6.94 (H₅ and H_{5'}, m, 2H). ¹⁹F NMR (282 MHz, CD₃CN): δ −59.62 (s), −59.72 (s), −63.00 (s), −72.94 (d, J_{F-31p} = 706.4 Hz). ¹³C NMR (75 MHz, CD₃CN): δ 165.98, 154.27, 151.80, 151.44, 150.96, 147.64, 144.36, 141.99, 140.57, 131.15, 126.83, 125.06, 122.08, 121.95. HRMS (ESI): *m/z* calculated for [C₃₅H₁₉N₅F₁₂¹⁹³Ir − PF₆]⁺ 930.10726; found 930.10658.

Ir-bpz. [Ir(ppyCF₃)₂bpz]⁺PF₆[−] was obtained by using the synthetic procedure described above with 2,2'-bipyrazine as ligand L (8.7 mg, 0.055 mmol, 2.2 equiv), to give an orange powder (39.8 mg, 74% yield). ¹H NMR (500 MHz, CD₃CN): δ 9.75 (H₉ and H_{9'}, s, 2H),

8.77 (H₇ and H_{7'}, d, $J_{7(7')-8(8')} = 3.0$ Hz, 2H), 8.48 (H₁ and H_{1'}, s, 2H), 8.27 (H₃ and H_{3'}, dd, $J_{3(3')-4(4')} = 8.1$ Hz, $J_{3(3')-5(5')} = 1.2$ Hz, 2H), 7.88 (H₄ and H_{4'}, ddd, $J_{3(3')-4(4')} = 8.1$ Hz, $J_{4(4')-5(5')} = 7.3$ Hz, $J_{4(4')-6(6')} = 1.3$ Hz, 2H), 7.82 (H₂ and H_{2'}, s, 2H), 7.78 (H₈ and H_{8'}, d, $J_{7(7')-8(8')} = 3.0$ Hz, 2H), 7.31 (H₆ and H_{6'}, dd, $J_{5(5')-6(6')} = 5.6$ Hz and $J_{4(4')-6(6')} = 1.3$ Hz, 2H), 6.98 (H₅ and H_{5'}, ddd, $J_{4(4')-5(5')} = 7.3$ Hz, $J_{5(5')-6(6')} = 5.6$ Hz, and $J_{3(3')-5(5')} = 1.2$ Hz, 2H). ¹⁹F NMR (282 MHz, CD₃CN): δ -59.58 (s), -63.03 (s), -72.94 (d, $J_{9F-31P} = 706.4$ Hz). ¹³C NMR (75 MHz, CD₃CN): δ 165.70, 152.34, 151.54, 151.31, 149.20, 147.73, 144.97, 140.79, 125.40, 125.30, 125.26, 122.25. HRMS (ESI): *m/z* calculated for [C₃₄H₁₈N₆F₁₂¹⁹¹Ir - PF₆]⁺ 929.10018; found 929.10038.

Ir-TAP. [Ir(ppyCF₃)₂TAP]⁺PF₆⁻ was obtained by using the synthetic procedure described above with 1,4,5,8-tetraazaphenanthrene as ligand **L** (10.0 mg, 0.055 mmol, 2.2 equiv), to give an orange powder (34.6 mg, 63% yield). ¹H NMR (500 MHz, CD₃CN): δ 9.21 (H₇ and H_{7'}, d, $J_{7(7')-8(8')} = 2.6$ Hz, 2H), 8.57 (H₉ and H_{9'}, s, 2H), 8.52 (H₁ and H_{1'}, s, 2H), 8.24 (H₃ and H_{3'}, d, $J_{3(3')-4(4')} = 8.1$ Hz, 2H), 8.10 (H₈ and H_{8'}, d, $J_{7(7')-8(8')} = 2.6$ Hz, 2H), 7.87 (H₂ and H_{2'}, s, 2H), 7.78 (H₄ and H_{4'}, ddd, $J_{3(3')-4(4')} = 8.1$ Hz, $J_{4(4')-5(5')} = 7.6$ Hz, $J_{4(4')-6(6')} = 1.4$ Hz, 2H), 7.18 (H₆ and H_{6'}, dd, $J_{5(5')-6(6')} = 5.6$ Hz, $J_{4(4')-6(6')} = 1.4$ Hz, 2H), 6.75 (H₅ and H_{5'}, ddd, $J_{4(4')-5(5')} = 7.6$ Hz, $J_{5(5')-6(6')} = 5.6$ Hz, $J_{3(3')-5(5')} = 1.1$ Hz, 2H). ¹⁹F NMR (282 MHz, CD₃CN): δ -59.47 (s), -62.99 (s), -72.99 (d, $J_{9F-31P} = 706.2$ Hz). ¹³C NMR (75 MHz, CD₃CN): δ 165.59, 153.46, 153.37, 153.12, 151.51, 147.62, 147.31, 145.91, 140.74, 140.63, 134.45, 125.34, 125.27, 125.16, 122.15. HRMS (ESI): *m/z* calculated for [C₃₆H₁₈N₆F₁₂¹⁹¹Ir - PF₆]⁺ 953.10018; found 953.10020.

Photophysical Measurements. UV/vis absorption spectra were recorded on a Shimadzu UV-1700 instrument. Room-temperature fluorescence spectra were recorded on a Varian Cary Eclipse instrument. Luminescence intensity at 77 K was recorded on a FluoroLog3 FL3-22 from Jobin Yvon equipped with an 18 V 450 W xenon Short Arc lamp and an R928P photomultiplier, using an Oxford Instrument Optistat DN nitrogen cryostat controlled by an Oxford Intelligent Temperature Controller (ITCS03S) instrument. Luminescence lifetime measurements were performed after irradiation at λ 400 nm obtained by the second harmonic of a titanium:sapphire laser (picosecond Tsunami laser Spectra Physics 3950-M1BB+39868-03 pulse picker doubler) at a 80 kHz repetition rate. Fluotime 200 from AMS Technologies was used for the decay acquisition. It consists of a GaAs microchannel plate photomultiplier tube (Hamamatsu Model R3809U-50) followed by a time-correlated single photon counting system from Picoquant (PicoHarp300). The ultimate time resolution of the system is close to 30 ps. Luminescence decays were analyzed with FLUOFIT software available from Picoquant. Cyclic voltammetry was carried out in a one-compartment cell, using a glassy-carbon-disk working electrode (approximate area 0.03 cm²), a platinum-wire counter electrode, and an Ag/AgCl reference electrode (salt bridge: 3 mol L⁻¹ KCl/saturated AgCl). The potential of the working electrode was controlled by an Autolab PGSTAT 100 potentiostat through a PC interface. The cyclic voltammograms were recorded with a sweep rate of 300 mV s⁻¹ in dried acetonitrile (Acros, HPLC grade). Tetrabutylammonium perchlorate (0.1 M) was used as supporting electrolyte, and the samples were purged with nitrogen before each measurement.

Franck–Condon Analyses for Emission Spectra. Fitting of the steady-state photoluminescence spectra was made possible through Franck–Condon line shape analysis. After the wavelength abscissa values were converted to energy, the emission spectral data (multiplied by λ²) were renormalized and fitted using either eq 1 (at room temperature) or eq 2 (at 77 K). Both equations correspond to Franck–Condon line shape predictions taking into account either one or two vibration modes, respectively.

$$I(\tilde{\nu}) = \sum_{\nu_m=0}^{\infty} \left(\frac{E_0 - \nu_m \hbar \omega_m}{E_0} \right)^3 \frac{S_M^{\nu_m}}{\nu_m!} \times \exp \left\{ -4 \ln 2 \left[\frac{\tilde{\nu} - E_0 + \nu_m \hbar \omega_m}{\Delta \tilde{\nu}_{1/2}} \right]^2 \right\} \quad (1)$$

$$I(\tilde{\nu}) = \sum_{\nu_m=0}^{\infty} \sum_{\nu_n=0}^{\infty} \left[\left(\frac{E_0 - \nu_m \omega_m - \nu_n \hbar \omega_n}{E_0} \right)^4 \frac{S_M^{\nu_m} S_N^{\nu_n}}{\nu_m! \nu_n!} \times \exp \left\{ -4 \ln 2 \left[\frac{\tilde{\nu} - E_0 + \nu_m \hbar \omega_m + \nu_n \hbar \omega_n}{\Delta \tilde{\nu}_{1/2}} \right]^2 \right\} \right] \quad (2)$$

In these equations, ν_m and ν_n are the vibrational quantum numbers for the acceptor mode, S_M and S_N are the Huang–Rhys factors, also known as the coupling factors, $\hbar \omega_m$ and $\hbar \omega_n$ correspond to the vibrational energy spacing in the ground-state potential energy surface for the corresponding vibration mode, and E_0 corresponds to the energy difference between the ground and excited state potential surfaces. Luminescence spectra can be modeled using one or two vibration modes, which correspond to the dominant vibration mode or an average of vibration. Usually, transitions implying $\nu^* = 0$ to $\nu = 0-5$ are sufficient to fit the experimental data. These transitions are broadened thanks to a Gaussian distribution to take into account solvent effects; $\Delta \nu_{1/2}$ is the full-width at half-maximum of the broadening for the transition, and a normalization factor of $4 \ln 2$ is added to ensure that the integrated area corresponds to the intensity of the line that is broadened into a Gaussian distribution.

Theoretical Calculations. All calculations were performed with the Gaussian09,⁴⁶ revision E.0, suite of programs employing the DFT method, the Becke three-parameter hybrid functional, and the Lee–Yang–Parr gradient-corrected correlation functional (B3LYP).^{47–49} All elements except iridium were assigned the 6-31G*(d,p) basis set. The double- ζ quality SBKJC VDZ ECP basis set with an effective core potential was employed for the Ir ion.^{50–53} No imaginary frequencies were obtained when frequency calculations on optimized geometries were performed. GaussView 5.0.9,⁵⁴ GaussSum 3.0,⁵⁵ and Chemission 4.30⁵⁶ software were used for data analysis, visualization, and surface plots. All calculations were performed in a MeCN solution by using the polarized continuum solvation model, as implemented in Gaussian 09.^{57,58}

Photoreaction Conditions and Analyses. In a quartz round-bottom flask, Ir-pzpy and Ir-TAP (20 mL, 5×10^{-5} mol/L) in the presence of GMP (respectively 0.0125 and 0.0425 mol/L) were illuminated for 72 h, under an argon atmosphere with continuous stirring at room temperature, using six fluorescent black lights (F8T5-BLB (12 in.), 8 W). GMP was used as an internal buffer; the pH was adjusted between 6 and 7 by adding HCl. The photoreactions were followed by analytical HPLC-UV/vis and analyzed off-line by mass spectrometry. HPLC analyses were performed on a Waters Alliance 2690 instrument using a XBridge C18 column (50 × 4.6 mm; 2.5 μm) as the stationary phase. The elutions were performed with a gradient starting from 90/10 water/acetonitrile (0.1% TFA) to 10/90 water/acetonitrile (0.1% TFA). The nature and structure of the complexes after the photoreaction were assessed by matrix-assisted laser desorption/ionization time-of-flight mass spectrometry (MALDI-ToF-UMONS). MALDI-ToF mass spectra were recorded using a Waters QToF Premier mass spectrometer equipped with a Nd:YAG laser using the third harmonic with a wavelength of 355 nm. In the context of this study, a maximum output of ~65 J was delivered to the sample in 2.2 ns pulses at a 50 Hz repeating rate. Time-of-flight mass analyses were performed in the reflection mode. The matrix, *trans*-2-[3-(4-*tert*-butyl-phenyl)-2-methyl-2-propenylidene]malononitrile (DCTB), was prepared as a 40 mg/mL solution in chloroform. The matrix solution (1 μL) was applied to a stainless steel MALDI target and air-dried. Reaction mixtures were dissolved in acetonitrile to obtain 1 mg/mL solutions, and 1 μL aliquots of these solutions were

spotted onto the target area (already bearing the matrix crystals) and then air-dried.

RESULTS AND DISCUSSION

Synthesis and Characterization. The synthesis of the four Ir(III) complexes was achieved in two steps according to methodologies previously described for similar compounds.^{59,60} As shown in Chart 1, these complexes possess the same skeleton with two cyclometalated ligands bearing two trifluoromethyl groups but differ in the N^N coordinating ligand. They were unambiguously characterized by ¹H, ¹³C, and ¹⁹F NMR spectroscopy, high-resolution mass spectrometry (HRMS), X-ray crystal diffraction, and HPLC (Figures S1–S25 and Tables S1 and S2).

For all four Ir complexes **Ir-bpy**, **Ir-pzpy**, **Ir-bpz**, and **Ir-TAP**, crystals suitable for X-ray diffraction were grown from an acetonitrile/diethyl ether solution. Crystals were measured at room temperature except for **Ir-TAP** which was flash-cooled to 150 K prior to data collection. Crystallographic and refinement parameters are given in Table S1 in the Supporting Information along with additional refinement details.

The combination of three bidentate chelating ligands, two ppyCF₃ and one diimine ligand, results in discrete complexes with octahedral geometries around the Ir center. The chelating nitrogen atoms of the two ppyCF₃ ligands are arranged trans to one another with angles between the core ppy systems of 71.18° (**Ir-bpy**), 88.38/78.45°⁶¹ (**Ir-pzpy**), 79.57° (**Ir-bpz**), and 73.88° (**Ir-TAP**). As a result of the trans arrangement of the ppyCF₃ ligands, the complexes show a pseudo-2-fold symmetry with the 2-fold axes passing through the middle of the diimine ligand. The centrosymmetric nature of the space groups the complexes crystallized in indicates that both Λ and Δ enantiomers are present. For the structure of **Ir-pzpy**, the combination of the positional disorder in the asymmetric pzpy ligand and the observed disorder of one of the ppyCF₃ ligands results in four possible arrangements of the ligands around the Ir atom, which all cocrystallize in the same asymmetric unit (see the Supporting Information for more details on the observed disorder).

The positively charged complexes are counterbalanced by an isolated PF₆[−] anion.

Searches in the CSD database (version 5.38 + 3 updates), reveal a significant curvature (Figure S21) for unsubstituted ppy ligands, which are principally found as bidentate chelating ligands. The curvature is calculated as the angle between the centroids of the aromatic rings and the bond between them. Over a 163.7–179.5° range, the mean value is found to be 173.7°. Substituents in the 3- and 5-positions of the phenyl moiety induce no effect on this average, and it is also not influenced by substitutions at position 6. The rotation between the phenyl and pyridine rings, as defined by the torsion angle, involving the coordinating atoms and the carbon atoms on either side of the linking bond, is about 0°, showing no twist between the aromatic rings. The reported structures do not deviate from the literature values in terms of curvature (Table S2).

Photophysical Properties. Electrochemistry. To get information on the relative energies of their HOMO and LUMO levels, the redox potentials of the four complexes were determined by cyclic voltammetry in dry deoxygenated acetonitrile (Table 1). For comparison purposes, the electrochemical data of [Ir(ppy)₂bpy]⁺ are also gathered in the table. For this complex, the first oxidation and reduction waves are

Table 1. Electrochemical Data for [Ir(ppy)₂bpy]⁺ (Ir-bpy), Ir-pzpy, Ir-bpz, and Ir-TAP)^a

complex	$E_{1/2}(\text{ox})/\text{V vs Ag/AgCl}$	$E_{1/2}(\text{red})/\text{V vs Ag/AgCl}$	
		1	2
[Ir(ppy) ₂ bpy] ⁺	1.30 (r)	−1.33 (r)	
Ir-bpy	>2	−1.11 (r)	
Ir-pzpy	>2	−0.82 (r)	−1.58 (r)
Ir-bpz	>2	−0.58 (r)	−1.31 (r)
Ir-TAP	>2	−0.60 (r)	−1.29 (r)

^aElectrochemical data were recorded at room temperature in dry deoxygenated acetonitrile with Bu₄NClO₄ 0.1 M as supporting electrolyte; r = reversible.

usually attributed to the oxidation of the Ir-phenylpyridine moiety and the reduction of the bipyridine, respectively.^{36,59} The data obtained for the four novel complexes are interpreted along the same train of thought; indeed, no oxidation process can be detected before 2 V vs Ag/AgCl (Table 1 and Figures S26 and S27) due to the presence of trifluoromethyl groups on the cyclometalated ligand, which impoverish the electron density in the Ir-phenylpyridine moiety. Similar results have already been obtained for other Ir(III) complexes bearing the same carbometalated ppyCF₃ ligand and have been attributed to a large stabilization of the HOMO level by the electron-withdrawing fluorocarbons.^{42,62} In the reduction, the wave is attributed to a process involving the N^N ligand; the anodic shift observed from **Ir-bpy** to **Ir-pzpy** and to **Ir-bpz/TAP** is consistent with the presence of a first and a second nonchelating nitrogen added on the N^N ligand. The introduction of these nonchelating nitrogen atoms induces π deficiency of the N^N ligand, lowering the LUMO level and easing its reduction; **Ir-bpz** and **Ir-TAP**, each bearing two nonchelating nitrogens, are reduced at a similar potential (ca. −0.60 V vs Ag/AgCl).

Absorption Spectroscopy. The absorption spectra in MeCN at room temperature for the four complexes are depicted in Figure 1. The corresponding spectroscopic data, as well as data for the reference [Ir(ppy)₂bpy]⁺, are summarized in Table 2.

All complexes display intense absorption bands with high molar extinction coefficients ($\epsilon > 2 \times 10^4 \text{ M}^{-1} \text{ cm}^{-1}$) between 230 and 340 nm. By comparison with literature and UV spectra of the free ligands, these bands are assigned to ligand centered (LC) transitions. Charge transfer (CT) transitions can be

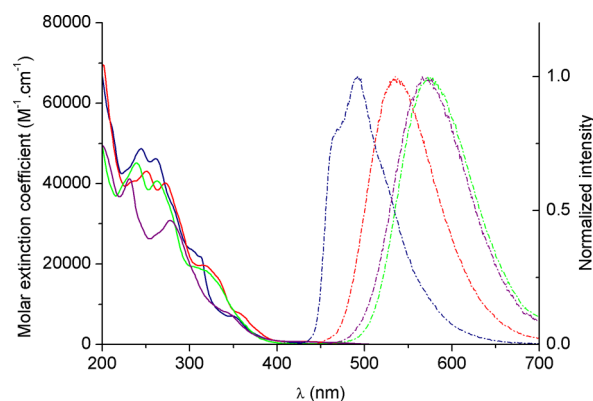


Figure 1. Absorption (solid lines) and emission (λ_{ex} 365 nm, dashed lines) spectra of **Ir-bpy** (blue), **Ir-pzpy** (red), **Ir-bpz** (green), and **Ir-TAP** (purple) measured in air at room temperature in MeCN.

Table 2. UV–Visible Absorption Data in Acetonitrile at 298 K for $[\text{Ir}(\text{ppy})_2\text{bpy}]^+$ (**Ir-bpy**, **Ir-pzpy**, **Ir-bpz**, and **Ir-TAP**)

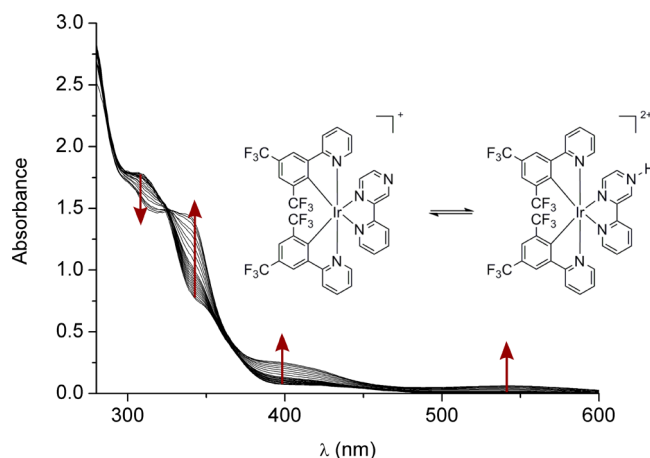
complex	$\lambda_{\text{max}}(\text{abs})/\text{nm}$ ($\epsilon/10^3 \text{ M}^{-1} \text{ cm}^{-1}$)
$[\text{Ir}(\text{ppy})_2\text{bpy}]^+$	257 (512), 267 (487), 310 (227), 339 (96), 376 (64), 412 (36), 467 (7)
Ir-bpy	247 (480), 263 (460), 306 (230), 314 (213), 353 (68), 423 (4)
Ir-pzpy	254 (425), 273 (401), 322 (191), 362 (70), 427 (7)
Ir-bpz	241 (450), 265 (404), 317 (184), 431 (3)
Ir-TAP	233 (407), 281 (305), 345 (77), 429 (7)

observed at lower energy ($\lambda > 340 \text{ nm}$). The nature of these transitions is not completely well defined; they correspond to a mixture of ligand to ligand (LLCT) and metal to ligand charge transfer (MLCT) transitions, involving the metal, the ppyCF_3 ligand as an electron donor, and the diimine ligand as an electron acceptor. As previously proposed in the literature, we rather consider these transition as metal–ligand to ligand charge transfer (MLLCT); indeed, on the basis of the cyclic voltammetry, a contribution of the whole Ir-ppyCF_3 fragment to the HOMO is suggested, supporting the MLLCT $d\pi_{\text{Ir-C}} \rightarrow \pi^*_{\text{N}^{\wedge}\text{N}}$ attribution.^{63,64} Bands from 340 to 400 nm arise probably from spin-allowed ¹MLLCT transitions ($\epsilon \approx (1-10) \times 10^3 \text{ M}^{-1} \text{ cm}^{-1}$) whereas the lowest-lying absorptions ($\lambda > 400 \text{ nm}$) are ascribed to spin-forbidden ³MLLCT transitions ($\epsilon < 1 \times 10^3 \text{ M}^{-1} \text{ cm}^{-1}$). The mixed spin character of these transitions is due to the strong spin–orbit coupling effect, which facilitates intersystem crossing between singlet and triplet states ($\xi_{\text{Ir}} = 4430 \text{ cm}^{-1}$).⁶⁵

Lowest-energy transitions for the four complexes appear at higher energy in comparison to the reference $[\text{Ir}(\text{ppy})_2\text{bpy}]^+$ (Table 2). As explained previously, this effect is attributed to the stabilization of the HOMO level by electron-withdrawing fluorocarbons on the cyclometalated ligand. It is also worth mentioning that the anodic shift, observed in reduction upon addition of one or two nonchelating nitrogen atoms, results in a shorter gap between the HOMO and LUMO. Consequently, the lowest energy transitions of **Ir-TAP** and **Ir-bpz** are slightly red shifted in comparison to those of **Ir-pzpy** and **Ir-bpy** (Table 2).

This stabilization effect on the LUMO level can be further strengthened upon protonation of one nonchelating nitrogen atom of **Ir-pzpy**, **Ir-bpz**, and **Ir-TAP** by addition of sulfuric acid in acetonitrile (Figure 2 and Figures S28 and S29). The protonation of the nonchelating nitrogen of **Ir-pzpy** induces modifications of the UV–visible spectrum of the complex (Figure 2); the presence of an isosbestic point ($\lambda 330 \text{ nm}$) indicates that two species are in equilibrium: the protonated and the nonprotonated forms. As expected, the protonated form of **Ir-pzpy** is characterized by a new absorption band at lower energy (around 540 nm). This bathochromic shift of the lowest-lying energy transitions results from the strong stabilization of the LUMO centered on the pzpy ligand after protonation. Similar results have been obtained for **Ir-bpz** and **Ir-TAP** with new bands, respectively, at around 560 and 565 nm (Figures S28 and S29), confirming the $\text{N}^{\wedge}\text{N}$ ligand character of the LUMO.⁶⁶

Emission Spectroscopy. Emission data in acetonitrile at room temperature (Table 3) are in good agreement with cyclic voltammetry and absorption analyses. As expected, emission maxima of all complexes appear at higher energy in comparison to the reference $[\text{Ir}(\text{ppy})_2\text{bpy}]^+$ and are affected by the number of nonchelating nitrogen atoms present in the $\text{N}^{\wedge}\text{N}$ ligand.

**Figure 2.** Absorption spectral changes for a solution of **Ir-pzpy** in MeCN at room temperature for increasing concentrations of sulfuric acid (0, 0.05, 0.094, 0.139, 0.162, 0.184, 0.207, 0.229, 0.251, 0.273, 0.294, 0.316, 0.337, 0.400, 0.461, 0.541, 0.618, 0.712, 0.821, 0.925, and 1.041 M).

Each time one nitrogen atom is added on the diimine ligand, the emission band is red-shifted by ca. 40 nm. The CT nature of the excited state of the four complexes is confirmed by the large k_{r} values ($>10^4 \text{ s}^{-1}$) and the blue shift of the emission band at 77 K (Table 3 and Figure S30). Interestingly, whereas the broad and structureless emission spectra also support the MLLCT assignment for **Ir-pzpy**, **Ir-bpz**, and **Ir-TAP**, the emission spectrum of **Ir-bpy** displays structural features, generally witnessing some LC character of the transition (Figure 1). This kind of behavior was previously discussed by Zanoni et al.⁶⁷ for a similar complex, $[\text{Ir}(\text{Fppy})_2\text{dmb}]^+$ (Fppy = 2-(2,4-difluorophenyl)pyridine; dmb = 4,4'-dimethyl-2,2'-bipyridine). This Ir(III) complex, bearing electron-withdrawing groups on the ppy ligands, is characterized by a mixed ³LC–³MLLCT excited state, where the LC is a transition centered on the bpy ligand. The ratio LC/MLLCT depends on the temperature, due to the sensitivity of the MLLCT excited state to the medium. In a frozen medium, a rigidochromic effect exists and is marked by the inability of the surrounding medium to stabilize the dipole of the CT transitions.^{68,69} Therefore, emission from this kind of excited state appears at higher energy at 77 K in comparison to that at 298 K. In contrast, LC excited states are almost unaffected thanks to their low dipole character. Consequently, the contribution of the LC to the excited state of $[\text{Ir}(\text{Fppy})_2\text{dmb}]^+$ is minor at 298 K but is predominant at 77 K. We have therefore investigated whether some LC character could be found in the excited state at room temperature.

Franck–Condon Analyses of Emission Spectra at 298 and 77 K. The participation of a LC transition in the emissive excited state of the four complexes was investigated through Franck–Condon line-shape analysis of the emission spectra. Fitting of the experimental spectra in acetonitrile at 298 K was realized using an average vibration mode approximation (eq 1).⁷¹ The emission spectral fitting parameters are given in Table 4. The experimental and calculated spectra are compared in Figure 3.

The $h\nu_{\text{m}}$ values for the four complexes were evaluated at $\sim 1200 \text{ cm}^{-1}$ (Table 4), consistent with results previously obtained for other Ru(II), Os(II), and Ir(III) polypyridine complexes.^{67,71,72} This vibration mode is ascribed to ring-

Table 3. Emission Data in Acetonitrile at 298 K and in EtOH/MeOH (4/1) at 77 K for [Ir(ppy)₂bpy]⁺ (Ir-bpy, Ir-pzpy, Ir-bpz, and Ir-TAP)

complex	$\lambda_{\max}(\text{em})/\text{nm}$		τ/ns (MeCN, 298 K)		Φ^c (MeCN, 298 K)		$k_r/10^3 \text{ s}^{-1}$
	MeCN ^a	77 K ^b	air	Ar	air	Ar	
[Ir(ppy) ₂ bpy] ⁺	599	515	63	307	0.017	0.035	114.0
Ir-bpy	493	457	665	2144	0.060	0.108	50.4
Ir-pzpy	539	507	1036	1513	0.116	0.133	87.9
Ir-bpz	579	515	496	590	0.087	0.104	176.3
Ir-TAP	574	512	795	1121	0.102	0.154	137.4

^aIn acetonitrile at 298 K (λ_{ex} 365 nm). ^bIn 4/1 EtOH/MeOH at 77 K (λ_{ex} 365 nm). ^cMeasured relative to quinine ($\Phi_{\text{ref}} = 0.546$ in 0.5 M H₂SO₄ in water⁷⁰) (λ_{ex} 366 nm).

Table 4. Emission Parameters for the Different Complexes Evaluated by Franck–Condon Line-Shape Analysis of Emission Spectra in Acetonitrile at 298 K According to Eq 1

	E_0/cm^{-1} [nm]	$h\omega_m/\text{cm}^{-1}$	S_M	$\Delta\nu_{1/2}/\text{cm}^{-1}$
Ir-bpy	21429 [467]	1181	1.64	1254
Ir-pzpy	19019 [526]	1182	0.92	2269
Ir-bpz	17591 [568]	1192	0.68	2332
Ir-TAP	17670 [566]	1181	0.57	2585

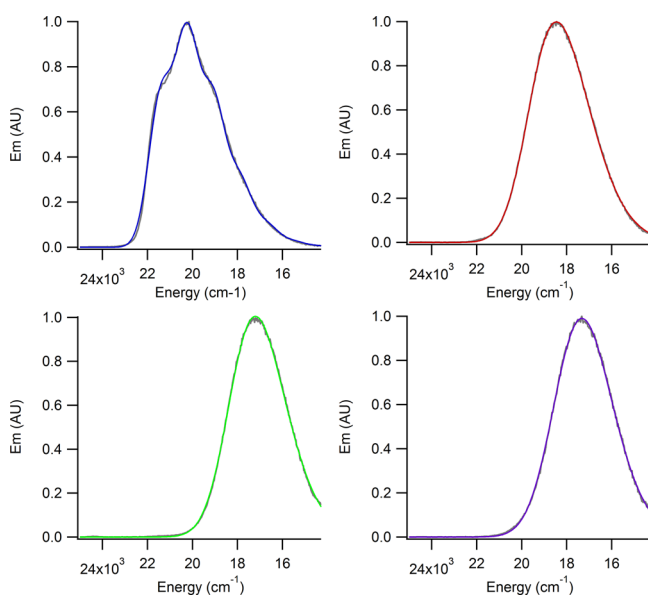


Figure 3. Emission spectra in acetonitrile at 298 K (gray) and fitted data (color) of **Ir-bpy** (blue), **Ir-pzpy** (red), **Ir-bpz** (green), and **Ir-TAP** (purple).

stretching vibrations in the N[^]N acceptor ligand. Moreover, **Ir-pzpy**, **Ir-bpz**, and **Ir-TAP** are characterized by large bandwidths at half-height (2200–2600 cm⁻¹) similar to previously described MLLCT Ir(III) emitters.⁶⁷ In contrast, $\Delta\nu_{1/2}$ is much lower for **Ir-bpy** (1254 cm⁻¹), probably due to a mixed LC-MLLCT nature of its excited state.

Further investigations were carried out by Franck–Condon analyses of the emission spectra of the four complexes and the free ligands at 77 K. In this case, a model with two vibration modes, described in the literature by Meyer and Woodruff,⁷¹ was used (eq 2). The experimental and fitted spectra of the complexes are shown in Figure 4. The emission spectral fitting parameters are summarized in Table 5, as well as data for the free ligands for comparison purposes. The experimental and simulated spectra of the free ligands at 77 K are available in Figure S31 in the Supporting Information.

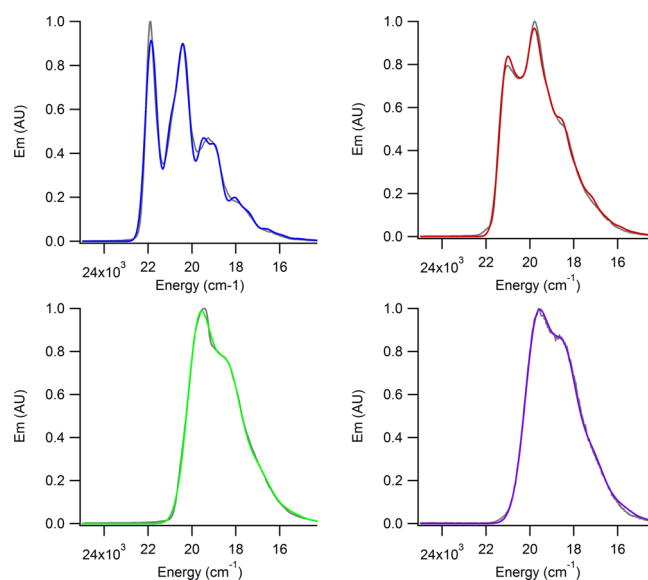


Figure 4. Emission spectra in EtOH/MeOH (4/1) at 77 K (gray) and fitted data (color) of **Ir-bpy** (blue), **Ir-pzpy** (red), **Ir-bpz** (green), and **Ir-TAP** (purple).

The band energy blue shifts of $\sim 2200 \text{ cm}^{-1}$ for **Ir-pzpy**, **Ir-bpz**, and **Ir-TAP** at 77 K in comparison to room temperature agree with the MLLCT character of their excited state (Tables 4 and 5). As expected, the hypsochromic shift is far less intense ($\sim 400 \text{ cm}^{-1}$) for **Ir-bpy** due to the participation of a LC transition to the emissive state. A medium-frequency vibrational mode, $h\omega_m$, was estimated in the range 1250–1450 cm⁻¹ for all complexes, consistent with ring vibrations in the diimine ligand⁷³ (Table 5). The low-frequency vibrational mode, $h\omega_n$, arises from Ir–N stretching modes; its value for **Ir-bpz** and **Ir-TAP** ($\sim 375 \text{ cm}^{-1}$) is similar to those for previously studied Ir(III) complexes⁶⁷ and confirms the MLLCT character of their emissive state. The last two complexes show particular structural features. The $h\omega_n$ and $\Delta\nu_{1/2}$ values for both compounds are more comparable to spectral parameters obtained for free ligands at 77 K (Table 5). This effect is clearly indicative of the participation of a LC excited state in emission. Similarly to the complex described by Zanoni et al.,⁶⁷ **Ir-pzpy** is characterized by an inversion in excited-state ordering, with emission from MLLCT at 298 K and LC at 77 K. In the case of **Ir-bpy**, the emissive state is a mixed LC-MLLCT excited state at 298 K. When the temperature is lowered, the contribution of the LC increases while the MLLCT proportion decreases.

In conclusion, all complexes emit from a ³MLLCT excited state in acetonitrile at room temperature, with the participation

Table 5. Emission Parameters for the Different Complex and Free Ligands Evaluated by Franck–Condon Line-Shape Analysis of Emission Spectra in EtOH/MeOH (4/1) at 77 K According to Eq 2

	E_0/cm^{-1} [nm]	$h\omega_m/\text{cm}^{-1}$	S_M	$h\omega_n/\text{cm}^{-1}$	S_N	$\Delta\nu_{1/2}/\text{cm}^{-1}$
Ir-bpy	21860 [457]	1454	1.13	883	0.61	629
Ir-pzpy	21101 [474]	1301	1.12	624	0.84	735
Ir-bpz	19922 [502]	1367	0.85	381	1.07	1111
Ir-TAP	19756 [506]	1263	1.01	370	0.32	1274
ppyCF ₃	22909 [437]	1419	1.35	859	1.17	719
bpy	23347 [428]	1445	1.47	858	1.20	645
pzpy	22732 [440]	1401	1.10	834	1.50	656
bpz	22305 [448]	1389	0.94	823	1.61	652
TAP	21581 [463]	1384	1.40	578	1.04	647

of a ³LC state centered on the bpy or ppyCF₃ ligand in the case of Ir-bpy. In frozen medium, Ir-bpz and Ir-TAP remain emissive from the ³MLLCT excited state, whereas the nature of the emissive excited state of Ir-bpy and Ir-bpy is modified and becomes mainly ³LC in character.

Time-Dependent Density Functional Theory Calculations. Computational studies were performed to confirm the proposed assignment after experimental analyses and to get more information on the energy gap between ³MLLCT and ³LC states for the four complexes.

The ground and vertical excited state electronic structures were investigated by means of DFT/TD-DFT calculations using the B3LYP method.^{47–49} All elements except iridium were assigned the 6-31G*(d,p) basis set. The double- ζ -quality SBKJC VDZ ECP basis set with an effective core potential was employed for the Ir ion.^{50–53} Solvent (MeCN) was included by a polarizable continuum model (CPCM). Details on electronic and geometrical structures can be found in Figures S32–S42 and Tables S3–S23 in the Supporting Information.

All complexes show a mixed $d\pi_{\text{Ir}}-\pi_{\text{ppyCF}_3}$ HOMO, while the LUMO is largely centered on the diimine ligand (Tables S3, S6, S12, and S18). The lowest-energy spin-allowed transitions for all complexes are HOMO \rightarrow LUMO transitions and are consequently MLLCT in character (Table 6). Absorption spectra of the different complexes match very well with calculated singlet transitions (Figures S33, S35, S38, and S41). Moreover, the estimated S_1 energies vary with the number of nonchelating nitrogens, as observed experimentally in UV–visible spectroscopy and cyclic voltammetry (Figure 5). The effect of protonation was also well-reproduced by theoretical studies. The protonation induces a strong stabilization of the LUMO level for complexes with at least one nonchelating nitrogen (Figure 5). Consequently, their lowest-energy spin-allowed transition is red-shifted, following the same trend as experimental titrations.

The five lowest-energy triplet transitions were also calculated for the four complexes. As shown in Table 6, the lowest-energy spin-forbidden transitions are ³MLLCT in character for Ir-pzpy, Ir-bpz, and Ir-TAP. In contrast, the T_1 state of Ir-bpy is a mixed excited state, involving mainly a ³MLLCT character but also a LC transition centered on the ppyCF₃ ligand. This result is in good agreement with structural features identified in emission for this complex in acetonitrile at 298 K. In addition to the T_1 state, each complex is characterized by another triplet state ascribed to mainly a LC transition centered on the diimine ligand (Table 6). Through the series Ir-bpy, Ir-pzpy, Ir-TAP, and Ir-bpz, the energy gap between this state and T_1 increases. Therefore, this triplet state is close in energy to T_1 for Ir-bpy and Ir-pzpy, explaining the increasing LC character of their

Table 6. Selected Singlet and Triplet Transitions from TD-DFT Calculations for the Four Complexes in the Singlet Ground State (PBE0, LANL2DZ, CPCM; MeCN)

complex	excited state	energy/eV [nm]	major transition	character
Ir-bpy	S_1	2.94 [419]	H \rightarrow L (98%)	¹ MLLCT _{bpy}
	T_1	2.89 [427]	H \rightarrow L (46%)	³ MLLCT _{bpy}
			H \rightarrow L+2 (18%)	³ MLCT _{ppy} + ³ LC _{ppy}
			H-1 \rightarrow L+1 (14%)	³ LC _{ppy}
T_4	3.00 [411]	H-5 \rightarrow L (46%) H-3 \rightarrow L (19%) H \rightarrow L (15%)	³ LC _{bpy} ³ MLLCT _{bpy} ³ MLLCT _{bpy}	
Ir-pzpy	S_1	2.64 [467]	H \rightarrow L (98%)	¹ MLLCT _{pzpy}
	T_1	2.64 [471]	H \rightarrow L (97%)	³ MLLCT _{pzpy}
	T_2	2.89 [429]	H-6 \rightarrow L (46%) H-3 \rightarrow L (21%) H-4 \rightarrow L (13%)	³ LC _{pzpy} ³ MLLCT _{pzpy} ³ MLLCT _{pzpy}
Ir-bpz	S_1	2.42 [509]	H \rightarrow L (99%)	¹ MLLCT _{bpz}
	T_1	2.39 [516]	H \rightarrow L (98%)	³ MLLCT _{bpz}
	T_2	2.79 [443]	H-6 \rightarrow L (43%) H-4 \rightarrow L (26%) H-3 \rightarrow L (19%)	³ LC _{bpz} ³ MLLCT _{bpz} ³ MLLCT _{bpz}
Ir-TAP	S_1	2.47 [500]	H \rightarrow L (99%)	¹ MLLCT _{TAP}
	T_1	2.44 [506]	H \rightarrow L (97%)	³ MLLCT _{TAP}
	T_3	2.71 [455]	H-6 \rightarrow L+1 (44%) H-2 \rightarrow L+1 (11%)	³ LC _{TAP} ³ MLLCT _{TAP}

emissive state at 77 K. However, for the last two complexes, the energy gap between the two triplet states are too large to observe an inversion in excited-state ordering at low temperature as found for Ir-pzpy.

Photo-Oxidant and Photoreductant Behavior. The ability of the four complexes to abstract or give, under light irradiation, an electron was investigated by luminescence quenching experiments in the presence of redox-active species. Actually, we performed in acetonitrile steady-state luminescence titration experiments in the presence of 1,4-hydroquinone (HQ) or 1,4-benzoquinone (BQ). A pure dynamic quenching of the luminescence of the four complexes occurs upon the addition of HQ (Figure S43), consistent with a photo-oxidation of the HQ electron donor by the excited complexes. The quenching rate constants are reported in Table 7. These values are close to the limit of diffusion and indicate that oxidative quenching is very efficient, in agreement with the reduction potential of the excited complexes (Table 7).

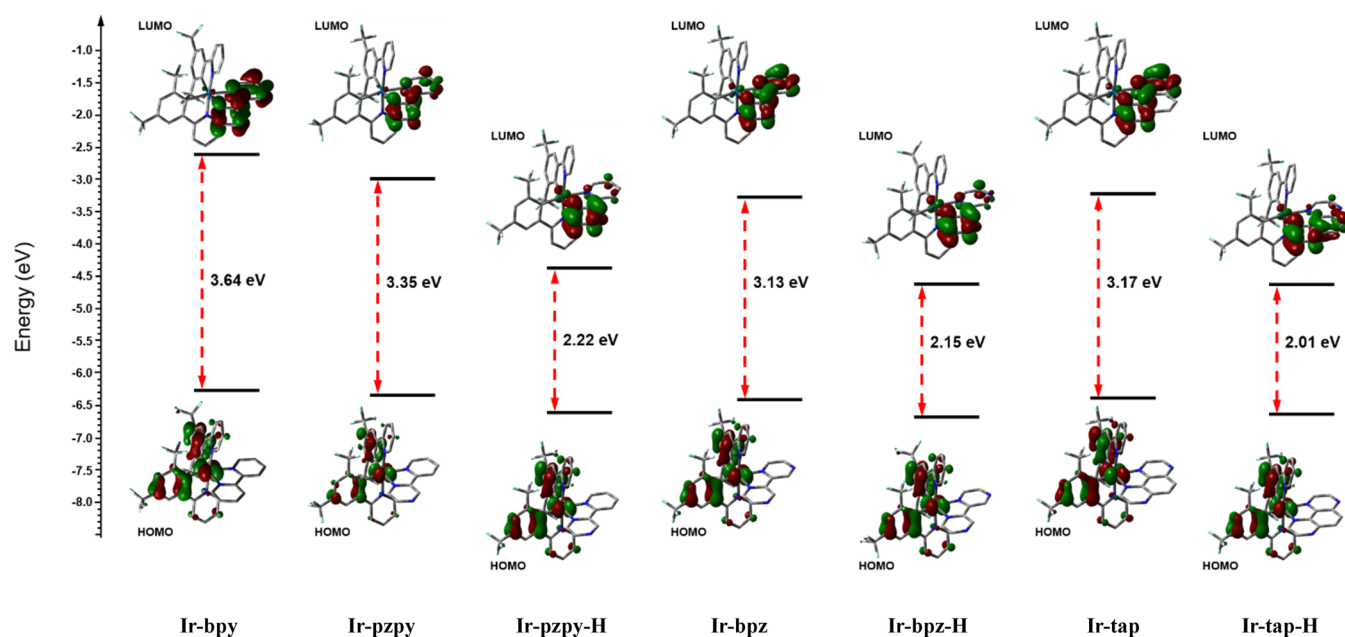


Figure 5. Comparison of the frontier molecular orbitals of the Ir(III) complexes with their HOMO–LUMO gap.

Table 7. Thermodynamic and Kinetic Parameters of the PET between the Four Complexes and BQ or HQ in MeCN

complex	$E_{\text{red}}^{*a}/\text{V}$	$k_{\text{q}}(\text{HQ})^b/10^9 \text{ s}^{-1}$	$E_{\text{ox}}^{*a}/\text{V}$	$k_{\text{q}}(\text{BQ})^c/10^9 \text{ s}^{-1}$	$K_{\text{s}}(\text{BQ})^c/\text{M}^{-1}$
Ir-bpy	+1.41	2.04	>−0.51	9.73	74.0
Ir-pzpy	+1.48	2.94	>−0.30	9.25	189.1
Ir-bpz	+1.56	8.10	>−0.14	9.32	129.0
Ir-TAP	+1.56	3.38	>−0.16	1.10	322.2

^a $E_{\text{red}}^{*} = E_{\text{red}} + E^{0-0}$ ($E^{0-0} = \pm hc/\lambda_{\text{em}}$); $E_{\text{ox}}^{*} = E_{\text{ox}} - E^{0-0}$ ($E^{0-0} = \pm hc/\lambda_{\text{em}}$).⁷⁵ ^bThe quenching rate constant, $k_{\text{q}}(\text{HQ})$, was obtained by using the Stern–Volmer equation $I_0/I = 1 + k_{\text{q}}\tau_0[\text{HQ}]$,⁷⁶ where I_0 is the intensity of the luminescence at the maximum of emission in the absence of a quencher, here HQ, I is the intensity of the luminescence at the maximum of emission in the presence of HQ, and τ_0 is the excited state lifetime of the complex in the absence of HQ. ^cIn the case of titration with BQ, a deviation in the linear Stern–Volmer relationship is observed. An association between BQ and the Ir(III) complex in the ground state due to a static quenching process causes this deviation. This association is probably due to π – π interaction between BQ and one ligand of the Ir complex. The quenching rate constant $k_{\text{q}}(\text{BQ})$ and association constant $K_{\text{s}}(\text{BQ})$ were obtained by using the equation $I_0/I = 1 + (k_{\text{q}}\tau_0 + K_{\text{s}})[\text{BQ}] + k_{\text{q}}\tau_0K_{\text{s}}[\text{BQ}]^2$,⁷⁶ where I_0 is the intensity of the luminescence at the maximum of emission in the absence of a quencher, here BQ, I is the intensity of the luminescence at the maximum of emission in the presence of BQ, and τ_0 is the excited state lifetime of the complex in the absence of BQ.

Interestingly, an extinction of the luminescence can also be observed with BQ and can be attributed in this case to the reduction of the BQ electron acceptor, indicating that the four complexes are also photoreductants. It should be noted that, in this case, Stern–Volmer plots obtained with BQ deviate from linearity with upward curvatures (Figure S44). This kind of behavior, previously identified for the photoreduction of BQ by chlorophyll B,⁷⁴ is due to the presence of a small static quenching contribution caused by interactions between BQ and complexes in the ground state ($K_{\text{s}} \approx 10^2 \text{ M}^{-1}$; see Table 7); both dynamic and static quenching constants are reported in Table 7.

Similar steady-state quenching experiments were then carried out in aqueous buffer in the presence of deoxyguanosine-5'-monophosphate (dGMP). The luminescence of all complexes is quenched upon addition of an increasing amount of dGMP (Figure S45). Similarly to photo-oxidant Ru(II) complexes,²² a pure dynamic quenching of the excited state of each complex is suggested by the linear evolution of the Stern–Volmer plots (Figure 6). The quenching rate constants (k_{q}) close to the limit of diffusion ($\sim 10^9 \text{ M}^{-1} \text{ s}^{-1}$) agree with efficient quenching for the four compounds (Table 8).

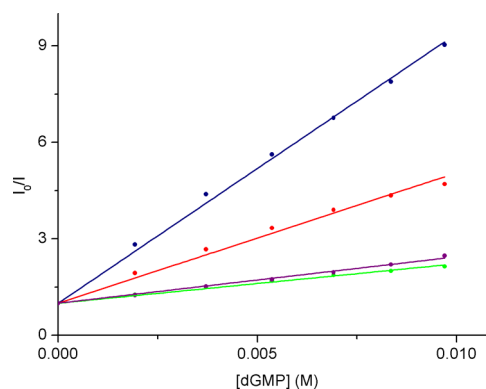


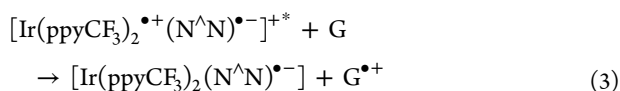
Figure 6. Stern–Volmer plots obtained upon the addition of dGMP to Ir-bpy (blue), Ir-pzpy (red), Ir-bpz (green), and Ir-TAP (purple). Measurements were made in TRIS-HCl 50 mM pH 7.4 (λ_{ex} 365 nm).

On the basis of the reduction potential of the excited complexes, we can safely assume that our four Ir(III) complexes are able to oxidize guanine under irradiation and thus that the extinction of luminescence is due to a photoinduced electron transfer (PET) from the nucleobase toward the excited complexes. Indeed, according to the empirical Rehm–Weller equation,⁷⁷ the PET is expected to be exergonic in the four cases (Table 8). Thus, the reaction between the two components can be resumed by eq 3.

Table 8. Thermodynamic and Kinetic Parameters of the PET between the Four Complexes and dGMP

	$E_{\text{red}}^{*a}/\text{V}$	$\Delta G_{\text{PET}}^b/\text{eV}$	τ_0^c/ns	$k_q^d/10^9 \text{ M}^{-1} \text{ s}^{-1}$
Ir-bpy	1.41	-0.37	1217	0.69
Ir-pzpy	1.39	-0.35	297	1.36
Ir-bpz	1.47	-0.43	74.4	1.65
Ir-TAP	1.44	-0.40	55.6	2.60

^a $E_{\text{red}}^{*} = E_{\text{red}} + E^{0-0}$ ($E^{0-0} = \pm hc/\lambda_{\text{em}}$). ^bExergonicity of the PET estimated by the Rhem–Weller equation $\Delta G = E_{\text{ox dGMP}} - E_{\text{red complex}} - E_{\text{complex}}^{0-0} - 0.06$ ($E_{\text{ox dGMP}} = 1.1 \text{ V}$).⁷⁸ $E^{0-0} = \pm hc/\lambda_{\text{em}}$. ^cMeasured in aerated water solution. ^dThe quenching rate constant, k_q , was obtained by using the Stern–Volmer equation $I_0/I = 1 + k_q\tau_0[\text{dGMP}]$,⁷⁶ where I_0 is the intensity of the luminescence at the maximum of emission in the absence of a quencher, here dGMP, I is the intensity of the luminescence at the maximum of emission in the presence of dGMP, and τ_0 is the excited state lifetime of the complex in the absence of dGMP.



Further evidence that an electron transfer occurs between excited Ir(III) complexes and guanine were obtained by continuous illumination of **Ir-pzpy** and **Ir-TAP** in the presence of the DNA base in different conditions. The results of these photoreactions were analyzed by HPLC-UV/vis and mass spectrometry.

First, we verified that the complexes remain stable under irradiation; complexes irradiated in solution in the absence of redox quencher do not degrade or induced the formation of any photoproduct (Figure S46). In contrast, when **Ir-pzpy** is irradiated in the presence of GMP, several new peaks are detected in HPLC (Figure S47) as well as by mass spectrometry with potentially some photoproduct derivatives. Indeed, after visible light irradiation, new signals at higher m/z are detected. Nevertheless, the photoproduct characterization is somewhat tricky. This is certainly due to the rich nature of the photophysics of Ir(III) complexes, in which a manifold of excited states have to be taken into account and, in addition, can be involved in photocatalytic reactions. Among the products generated during the photoreaction of **Ir-pzpy** and GMP, we could detect a high-mass product in which two iridium centers are present, as confirmed upon MALDI-ToF analysis (Figure S48). A similar binuclear species is also detected upon continuous irradiation of a solution of **Ir-TAP** and GMP (Figure S49). In order to get more structural information, MS/MS analyses were undertaken. Tandem mass spectrometry investigation showed that both photoproducts (i.e., with **Ir-pzpy** and **Ir-TAP**) share some similar fragment ions when they are subjected to collision-induced dissociation experiments (MS/MS) (Figures S50 and S51). This result suggests that they present similar structures and thus are likely to arise from similar mechanisms of formation. Nevertheless, due to the small amount of products formed, their exact structure has still not been completely elucidated, since these photoadducts could not be analyzed by NMR. In contrast to photooxidant Ru-TAP/HAT based compounds which lead to the formation of a photoadduct either between the ruthenium complex and GMP or between two Ru complexes, photoproducts generated upon irradiation of photoreactive Ir(III) seem more to lead to Ir–Ir photoadducts.

It is also worth mentioning that the binuclear compounds are also detected when continuous irradiation of a solution of **Ir-pzpy** and hydroquinone in MeCN is performed (Figure S52). Therefore, we can safely assert that their synthesis requires the formation of a monoreduced complex. When GMP is the electron donor, long-lived guanine radical cations are then concomitantly generated upon light irradiation. Because the monoreduced complex is irreversibly and quickly trapped in a photoproduct Ir–Ir, a back-electron-transfer reaction between the monoreduced complex and the guanine radical cannot occur. This means that the oxidized guanine is available to react with other substrates and, in a biological context, that the radical character of the oxidized guanine will be transferred to DNA very efficiently, leading to irreversible damage to the genetic material of the targeted cell.⁷⁹ The present photo-reactivity studies pave the way toward in cellulo studies, for which we expect that our iridium complexes will depict remarkable phototriggered toxicity, even under hypoxic conditions.

CONCLUSION

Four new bis-cyclometalated Ir(III) complexes were prepared and unambiguously characterized by ¹H, ¹³C, and ¹⁹F NMR spectroscopy, high-resolution mass spectrometry (HRMS), and X-ray crystal diffraction.

The electrochemical and spectroscopic data are in full agreement with the computational results, which indicate that the lowest-lying absorption bands for all complexes correspond to mixed LLCT and MLCT transitions, termed MLLCT (i.e., CT from the whole ppyCF₃–Ir fragment toward the diimine ligand). For their emission, the excited state is mainly a ³MLLCT state in acetonitrile at 298 K, with a contribution of an LC transition centered on the ppyCF₃ ligand for **Ir-bpy**. At 77 K, the emissive state of **Ir-bpz** and **Ir-TAP** remains ³MLLCT in character, whereas the last two complexes show an inversion in excited-state ordering, with predominant ³LC_{NN} character. This inversion can be explained by the presence of two triplet states relatively close in energy for these compounds. The two states, respectively largely ³MLLCT in character and mainly ³LC_{NN}, are not affected in the same way by the rigidochromic effect at low temperature. The LC is almost unaffected, whereas the MLLCT is blue-shifted and becomes consequently higher in energy than the LC state. In the case of **Ir-bpz** and **Ir-TAP**, this differential stabilization effect also occurs but the initial energy gap between the two excited states is too large to observe an inversion in excited-state ordering.

Photoredox properties of the four complexes were then investigated through quenching of luminescence experiments. First, a photoinduced electron transfer was established between the excited complexes and respectively 1,4-hydroquinone and 1,4-benzoquinone. This result has great interest from the perspective of exploiting the four complexes in photocatalytic devices. Evidence of an oxidative PET was also obtained in the presence of dGMP, leading to the formation of a radical cation on the nucleobase. This phenomenon could be used for phototherapies due to dramatic effects caused on the DNA structure such as strand cleavage. Consequently, present studies pave the way toward in cellulo experiments, for which we expect that our iridium complexes will depict remarkable phototriggered toxicity, even in hypoxic medium.

■ ASSOCIATED CONTENT

● Supporting Information

The Supporting Information is available free of charge on the ACS Publications website at DOI: 10.1021/acs.inorgchem.7b02778.

¹H NMR, ¹³C NMR, ¹⁹F NMR, and 2D ¹H–¹H COSY spectra, HRMS data, X-ray crystal diffraction data, and cyclic voltammograms for complexes Ir-bpy, Ir-pzpy, Ir-bpz, and Ir-TAP, additional spectroscopic data and Franck–Condon analyses of emission spectra of free ligands at 77 K, computational study details including geometrical and electronic structures and detailed TD-DFT results, and data from quenching of luminescence experiments and photoreactions (PDF)

Accession Codes

CCDC 1583159–1583162 contain the supplementary crystallographic data for this paper. These data can be obtained free of charge via www.ccdc.cam.ac.uk/data_request/cif, or by emailing data_request@ccdc.cam.ac.uk, or by contacting The Cambridge Crystallographic Data Centre, 12 Union Road, Cambridge CB2 1EZ, UK; fax: +44 1223 336033.

■ AUTHOR INFORMATION

Corresponding Author

*E-mail for B.E.: Benjamin.Elias@uclouvain.be.

ORCID

Robin Bevernaegie: 0000-0003-1605-9253

Lionel Marcédis: 0000-0002-6324-477X

Garry S. Hanan: 0000-0001-6671-5234

Present Address

^{||}Engineering of Molecular NanoSystems, Université libre de Bruxelles (U.L.B.), 50 Av. F.D. Roosevelt, CP165/64, 1050 Bruxelles, Belgium.

Notes

The authors declare no competing financial interest.

■ ACKNOWLEDGMENTS

R.B., L.M., and B.E. gratefully acknowledge the Fonds National pour la Recherche Scientifique (F.R.S.-FNRS), the *Fonds pour la Formation à la Recherche dans l'Industrie et dans l'Agriculture* (F.R.I.A.), the *Région Wallonne*, the *Université catholique de Louvain*, and the *Prix Pierre et Colette Bauchau* for financial support. G.S.H. and B.L.-M. thank the Natural Sciences and Engineering Research Council (NSERC) of Canada. B.E. and G.S.H. thank the Québec-Wallonie foundation for financial support. The S²MOs laboratory acknowledges the Fonds de la Recherche Scientifique (FRS-FNRS) for its contribution to the acquisition of the Waters QToF Premier mass spectrometer and for continuing support. Laurent Collard is deeply thanked for his help in the HPLC analyses. Frédérique Loiseau is thanked for her scientific contribution.

■ REFERENCES

(1) Campagna, S.; Puntoriero, F.; Nastasi, F.; Bergamini, G.; Balzani, V. In *Photochemistry and Photophysics of Coordination Compounds I*; Balzani, V., Campagna, S., Eds.; Springer Berlin Heidelberg: Berlin, Heidelberg, 2007; pp 117–214.

(2) Cano-Yelo, H.; Deronzier, A. Photocatalysis of the Pschorr reaction by tris-(2,2[prime or minute]-bipyridyl)ruthenium(II) in the phenanthrene series. *J. Chem. Soc., Perkin Trans. 2* **1984**, 2, 1093–1098.

(3) Rousset, E.; Chartrand, D.; Ciofini, I.; Marvaud, V.; Hanan, G. S. Red-light-driven photocatalytic hydrogen evolution using a ruthenium quaterpyridine complex. *Chem. Commun.* **2015**, 51, 9261–9264.

(4) Rousset, E.; Ciofini, I.; Marvaud, V.; Hanan, G. S. Facile One-Pot Synthesis of Ruthenium(II) Quaterpyridine-Based Photosensitizers for Photocatalyzed Hydrogen Production. *Inorg. Chem.* **2017**, 56, 9515–9524.

(5) Schott, O.; Pal, A. K.; Chartrand, D.; Hanan, G. S. A Bisamide Ruthenium Polypyridyl Complex as a Robust and Efficient Photosensitizer for Hydrogen Production. *ChemSusChem* **2017**, 10, 4436–4441.

(6) Marcaccio, M.; Paolucci, F.; Paradisi, C.; Roffia, S.; Fontanesi, C.; Yellowlees, L. J.; Serroni, S.; Campagna, S.; Denti, G.; Balzani, V. Electrochemistry of Multicomponent Systems. Redox Series Comprising up to 26 Reversible Reduction Processes in Polynuclear Ruthenium(II) Bipyridine-Type Complexes. *J. Am. Chem. Soc.* **1999**, 121, 10081–10091.

(7) Denti, G.; Campagna, S.; Serroni, S.; Ciano, M.; Balzani, V. Decanuclear homo- and heterometallic polypyridine complexes: syntheses, absorption spectra, luminescence, electrochemical oxidation, and intercomponent energy transfer. *J. Am. Chem. Soc.* **1992**, 114, 2944–2950.

(8) Denti, G.; Serroni, S.; Campagna, S.; Ricevuto, V.; Balzani, V. Made-to-order control of the direction of electronic energy transfer in tetranuclear luminescent metal complexes. *Coord. Chem. Rev.* **1991**, 111, 227–236.

(9) Concepcion, J. J.; Jurss, J. W.; Brennaman, M. K.; Hoertz, P. G.; Patrocinio, A. O. T.; Murakami Iha, N. Y.; Templeton, J. L.; Meyer, T. J. Making Oxygen with Ruthenium Complexes. *Acc. Chem. Res.* **2009**, 42, 1954–1965.

(10) Hagfeldt, A.; Boschloo, G.; Sun, L.; Kloo, L.; Pettersson, H. Dye-Sensitized Solar Cells. *Chem. Rev.* **2010**, 110, 6595–6663.

(11) Nazeeruddin, M. K.; Zakeeruddin, S. M.; Lagref, J. J.; Liska, P.; Comte, P.; Barolo, C.; Viscardi, G.; Schenk, K.; Graetzel, M. Stepwise assembly of amphiphilic ruthenium sensitizers and their applications in dye-sensitized solar cell. *Coord. Chem. Rev.* **2004**, 248, 1317–1328.

(12) Gill, M. R.; Thomas, J. A. Ruthenium(ii) polypyridyl complexes and DNA-from structural probes to cellular imaging and therapeutics. *Chem. Soc. Rev.* **2012**, 41, 3179–3192.

(13) Komor, A. C.; Barton, J. K. The path for metal complexes to a DNA target. *Chem. Commun.* **2013**, 49, 3617–3630.

(14) Marcédis, L.; Moucheron, C.; Kirsch-De Mesmaeker, A. Ru-TAP complexes and DNA: from photo-induced electron transfer to gene photo-silencing in living cells. *Philos. Trans. R. Soc., A* **2013**, 371, 20120131.

(15) Friedman, A. E.; Chambron, J. C.; Sauvage, J. P.; Turro, N. J.; Barton, J. K. A molecular light switch for DNA: Ru(bpy)₂(dppz)₂²⁺. *J. Am. Chem. Soc.* **1990**, 112, 4960–4962.

(16) Chen, X.; Wu, J.-H.; Lai, Y.-W.; Zhao, R.; Chao, H.; Ji, L.-N. Targeting telomeric G-quadruplexes with the ruthenium(ii) complexes [Ru(bpy)₂(tpn)]²⁺ and [Ru(phen)₂(tpn)]²⁺. *Dalton Trans.* **2013**, 42, 4386–4397.

(17) Cao, Q.; Li, Y.; Freisinger, E.; Qin, P. Z.; Sigel, R. K. O.; Mao, Z.-W. G-quadruplex DNA targeted metal complexes acting as potential anticancer drugs. *Inorg. Chem. Front.* **2017**, 4, 10–32.

(18) Piraux, G.; Bar, L.; Abraham, M.; Lavergne, T.; Jamet, H.; Dejeu, J.; Marcédis, L.; Defrancq, E.; Elias, B. New Ruthenium-Based Probes for Selective G-Quadruplex Targeting. *Chem. - Eur. J.* **2017**, 23, 11872–11880.

(19) Lim, M. H.; Song, H.; Olmon, E. D.; Dervan, E. E.; Barton, J. K. Sensitivity of Ru(bpy)₂dppz₂²⁺ Luminescence to DNA Defects. *Inorg. Chem.* **2009**, 48, 5392–5397.

(20) Deraedt, Q.; Marcédis, L.; Auvray, T.; Hanan, G. S.; Loiseau, F.; Elias, B. Design and Photophysical Studies of Acridine-Based RuII Complexes for Applications as DNA Photoprobes. *Eur. J. Inorg. Chem.* **2016**, 2016, 3649–3658.

(21) Boynton, A. N.; Marcédis, L.; Barton, J. K. [Ru(Me₄phen)-2dppz]₂²⁺, a Light Switch for DNA Mismatches. *J. Am. Chem. Soc.* **2016**, 138, 5020–5023.

- (22) Deraedt, Q.; Marcelis, L.; Loiseau, F.; Elias, B. Towards mismatched DNA photoprobes and photoreagents: "elbow-shaped" Ru(II) complexes. *Inorg. Chem. Front.* **2017**, *4*, 91–103.
- (23) Kajouj, S.; Marcelis, L.; Lemaur, V.; Beljonne, D.; Moucheron, C. Photochemistry of ruthenium (II) complexes based on 1,4,5,8-tetraazaphenanthrene and 2,2'-bipyrazine: a comprehensive experimental and theoretical study. *Dalton Trans.* **2017**, *46*, 6623.
- (24) Kirsh-de Mesmaeker, A.; Maetens, D.; Nasielski-Hinkens, R. Photoelectrochemistry of a new ruthenium complex, the Ru(II)-tris-(1,4,5,8-tetraazaphenanthrene) dication. *J. Electroanal. Chem. Interfacial Electrochem.* **1985**, *182*, 123–132.
- (25) Kirsch-De Mesmaeker, A.; Jacquet, L.; Masschelein, A.; Vanhecke, F.; Heremans, K. Resonance Raman spectra and spectroelectrochemical properties of mono- and polymetallic ruthenium complexes with 1,4,5,8,9,12-hexaazatriphenylene. *Inorg. Chem.* **1989**, *28*, 2465–2470.
- (26) Jacquet, L.; Mesmaeker, A. K.-D. Spectroelectrochemical characteristics and photophysics of a series of RuII complexes with 1,4,5,8,9,12-hexaazatriphenylene: effects of polycomplexation. *J. Chem. Soc., Faraday Trans.* **1992**, *88*, 2471–2480.
- (27) Kelly, J. M.; McConnell, D. J.; OhUigin, C.; Tossi, A. B.; Mesmaeker, A. K.-D.; Masschelein, A.; Nasielski, J. Ruthenium polypyridyl complexes; their interaction with DNA and their role as sensitizers for its photocleavage. *J. Chem. Soc., Chem. Commun.* **1987**, 1821–1823.
- (28) Jacquet, L.; Kelly, J. M.; Mesmaeker, A. K.-D. Photoadduct between tris(1,4,5,8-tetraazaphenanthrene)ruthenium(II) and guanosine monophosphate—a model for a new mode of covalent binding of metal complexes to DNA. *J. Chem. Soc., Chem. Commun.* **1995**, 913–914.
- (29) Elias, B.; Kirsch-De Mesmaeker, A. Photo-reduction of polycyclic aromatic Ru(II) complexes by biomolecules and possible applications. *Coord. Chem. Rev.* **2006**, *250*, 1627–1641.
- (30) Marcélis, L.; Surin, M.; Lartia, R.; Moucheron, C.; Defrancq, E.; Kirsch-De Mesmaeker, A. Specificity of Light-Induced Covalent Adduct Formation between RuII Oligonucleotide Conjugates and Target Sequences for Gene Silencing Applications. *Eur. J. Inorg. Chem.* **2014**, *2014*, 3016–3022.
- (31) Marcélis, L.; Van Overstraeten-Schlögel, N.; Lambertmont, J.; Bontems, S.; Spinelli, N.; Defrancq, E.; Moucheron, C.; Kirsch-De Mesmaeker, A.; Raes, M. Light-Triggered Green Fluorescent Protein Silencing in Human Keratinocytes in Culture Using Antisense Oligonucleotides Coupled to a Photoreactive Ruthenium(II) Complex. *ChemPlusChem* **2014**, *79*, 1597–1604.
- (32) Marcélis, L.; Kajouj, S.; Ghesquière, J.; Fettweis, G.; Coupennie, I.; Lartia, R.; Surin, M.; Defrancq, E.; Piette, J.; Moucheron, C.; Kirsch-De Mesmaeker, A. Highly DNA-Photoreactive Ruthenium 1,4,5,8-Tetraazaphenanthrene Complex Conjugated to the TAT Peptide: Efficient Vectorization inside HeLa Cells without Phototoxicity - The Importance of Cellular Distribution. *Eur. J. Inorg. Chem.* **2016**, *2016*, 2902–2911.
- (33) Shao, F.; Elias, B.; Lu, W.; Barton, J. K. Synthesis and Characterization of Iridium(III) Cyclometalated Complexes with Oligonucleotides: Insights into Redox Reactions with DNA. *Inorg. Chem.* **2007**, *46*, 10187–10199.
- (34) Lo, K. K.-W.; Li, S. P.-Y.; Zhang, K. Y. Development of luminescent iridium(III) polypyridine complexes as chemical and biological probes. *New J. Chem.* **2011**, *35*, 265–287.
- (35) Lo, K. K.-W.; Zhang, K. Y. Iridium(III) complexes as therapeutic and bioimaging reagents for cellular applications. *RSC Adv.* **2012**, *2*, 12069–12083.
- (36) Flamigni, L.; Barbieri, A.; Sabatini, C.; Ventura, B.; Barigelletti, F. In *Photochemistry and Photophysics of Coordination Compounds II*; Balzani, V., Campagna, S., Eds.; Springer Berlin Heidelberg: Berlin, Heidelberg, 2007; pp 143–203.
- (37) Maestri, M.; Balzani, V.; Deuschel-Cornioley, C.; Zelewsky, A. V. Photochemistry and Luminescence of Cyclometalated Complexes. *Adv. Photochem.* **1992**, *1*–68.
- (38) Dixon, I. M.; Collin, J.-P.; Sauvage, J.-P.; Flamigni, L.; Encinas, S.; Barigelletti, F. A family of luminescent coordination compounds: iridium(III) polypyridine complexes. *Chem. Soc. Rev.* **2000**, *29*, 385–391.
- (39) *CrysAlisPro Software system, version 1.171.37.35*; Rigaku Corporation, Oxford, U.K., 2014.
- (40) Sheldrick, G. SHELXT - Integrated space-group and crystal-structure determination. *Acta Crystallogr., Sect. A: Found. Adv.* **2015**, *71*, 3–8.
- (41) Sheldrick, G. A short history of SHELX. *Acta Crystallogr., Sect. A: Found. Crystallogr.* **2008**, *64*, 112–122.
- (42) Shavaleev, N. M.; Monti, F.; Scopelliti, R.; Armaroli, N.; Grätzel, M.; Nazeeruddin, M. K. Blue Phosphorescence of Trifluoromethyl- and Trifluoromethoxy-Substituted Cationic Iridium(III) Isocyanide Complexes. *Organometallics* **2012**, *31*, 6288–6296.
- (43) Berghian, C.; Darabantu, M.; Turck, A.; Plé, N. Metallation of pyridin-2-yl diazines. Use of pyridine ring as ortho-directing group. Diazines. Part 45. *Tetrahedron* **2005**, *61*, 9637–9644.
- (44) Bouilly, L.; Turck, A.; Plé, N.; Darabantu, M. Aryl-aryl bonds formation in pyridine and diazine series. Diazines part 41. *J. Heterocycl. Chem.* **2005**, *42*, 1423–1428.
- (45) Nasielski-Hinkens, R.; Benedek-Vamos, M. Synthesis of di- and tetra-substituted 1,4,5,8-tetra-azaphenanthrenes (pyrazino[2,3-f]-quinoxalines). *J. Chem. Soc., Perkin Trans. 1* **1975**, *1*, 1229–1229.
- (46) Frisch, M. J.; Trucks, G. W.; Schlegel, H. B.; Scuseria, G. E.; Robb, M. A.; Cheeseman, J. R.; Scalmani, G.; Barone, V.; Mennucci, B.; Petersson, G. A.; Nakatsuji, H.; Caricato, M.; Li, X.; Hratchian, H. P.; Izmaylov, A. F.; Bloino, J.; Zheng, G.; Sonnenberg, J. L.; Hada, M.; Ehara, M.; Toyota, K.; Fukuda, R.; Hasegawa, J.; Ishida, M.; Nakajima, T.; Honda, Y.; Kitao, O.; Nakai, H.; Vreven, T.; Montgomery, J. A., Jr.; Peralta, J. E.; Ogliaro, F.; Bearpark, M. J.; Heyd, J. J.; Brothers, E. N.; Kudin, K. N.; Staroverov, V. N.; Kobayashi, R.; Normand, J.; Raghavachari, K.; Rendell, A. P.; Burant, J. C.; Iyengar, S. S.; Tomasi, J.; Cossi, M.; Rega, N.; Millam, J. M.; Klene, M.; Knox, J. E.; Cross, J. B.; Bakken, V.; Adamo, C.; Jaramillo, J.; Gomperts, R.; Stratmann, R. E.; Yazyev, O.; Austin, A. J.; Cammi, R.; Pomelli, C.; Ochterski, J. W.; Martin, R. L.; Morokuma, K.; Zakrzewski, V. G.; Voth, G. A.; Salvador, P.; Dannenberg, J. J.; Dapprich, S.; Daniels, A. D.; Farkas, O.; Foresman, J. B.; Ortiz, J. V.; Cioslowski, J.; Fox, D. J. *Gaussian 09, revision E.01*; Gaussian, Inc., Wallingford, CT, 2009.
- (47) Miehlich, B.; Savin, A.; Stoll, H.; Preuss, H. Results obtained with the correlation energy density functionals of Becke and Lee, Yang and Parr. *Chem. Phys. Lett.* **1989**, *157*, 200–206.
- (48) Becke, A. D. Density-functional thermochemistry. III. The role of exact exchange. *J. Chem. Phys.* **1993**, *98*, 5648–5652.
- (49) Lee, C.; Yang, W.; Parr, R. G. Development of the Colle-Salvetti correlation-energy formula into a functional of the electron density. *Phys. Rev. B: Condens. Matter Mater. Phys.* **1988**, *37*, 785–789.
- (50) Stevens, W. J.; Krauss, M.; Basch, H.; Jasien, P. G. Relativistic compact effective potentials and efficient, shared-exponent basis sets for the third-, fourth-, and fifth-row atoms. *Can. J. Chem.* **1992**, *70*, 612–630.
- (51) Cundari, T. R.; Stevens, W. J. Effective core potential methods for the lanthanides. *J. Chem. Phys.* **1993**, *98*, 5555–5565.
- (52) Stevens, W. J.; Basch, H.; Krauss, M. Compact effective potentials and efficient shared-exponent basis sets for the first- and second-row atoms. *J. Chem. Phys.* **1984**, *81*, 6026–6033.
- (53) Binkley, J. S.; Pople, J. A.; Hehre, W. J. Self-consistent molecular orbital methods. 21. Small split-valence basis sets for first-row elements. *J. Am. Chem. Soc.* **1980**, *102*, 939–947.
- (54) Dennington, R.; Keith, J. A.; Millam, J. M. *GaussView, version 5.0.9*; Gaussian Inc., Shawnee Mission, KS, 2009.
- (55) O'Boyle, N. M.; Tenderholt, A. L.; Langner, K. M. cclib: A library for package-independent computational chemistry algorithms. *J. Comput. Chem.* **2008**, *29*, 839–845.
- (56) Skripnikov, L. *Chemissian, version 4.30*; Chemissian, 2005–2016.
- (57) Miertuš, S.; Scrocco, E.; Tomasi, J. Electrostatic interaction of a solute with a continuum. A direct utilization of AB initio molecular potentials for the prevision of solvent effects. *Chem. Phys.* **1981**, *55*, 117–129.

- (58) Tomasi, J.; Mennucci, B.; Cammi, R. Quantum Mechanical Continuum Solvation Models. *Chem. Rev.* **2005**, *105*, 2999–3094.
- (59) Deraedt, Q.; Loiseau, F.; Elias, B. Photochemical Tuning of Tris-Bidentate Acridine- and Phenazine-Based Ir(III) Complexes. *J. Fluoresc.* **2016**, *26*, 2095–2103.
- (60) Lentz, C.; Schott, O.; Auvray, T.; Hanan, G.; Elias, B. Photocatalytic Hydrogen Production Using a Red-Absorbing Ir(III)–Co(III) Dyad. *Inorg. Chem.* **2017**, *56*, 10875.
- (61) For Ir-pzpy, one of the ppyCF₃ ligands is fully disordered, where both parts are found more or less parallel to each other.
- (62) Coppo, P.; Plummer, E. A.; De Cola, L. Tuning iridium(III) phenylpyridine complexes in the “almost blue” region. *Chem. Commun.* **2004**, 1774–1775.
- (63) Tamayo, A. B.; Garon, S.; Sajoto, T.; Djurovich, P. I.; Tsyba, I. M.; Bau, R.; Thompson, M. E. Cationic Bis-cyclometalated Iridium(III) Diimine Complexes and Their Use in Efficient Blue, Green, and Red Electroluminescent Devices. *Inorg. Chem.* **2005**, *44*, 8723–8732.
- (64) Volpi, G.; Garino, C.; Salassa, L.; Fiedler, J.; Hardcastle, K. L.; Gobetto, R.; Nervi, C. Cationic Heteroleptic Cyclometalated Iridium Complexes with 1-Pyridylimidazo[1,5- α]pyridine Ligands: Exploitation of an Efficient Intersystem Crossing. *Chem. - Eur. J.* **2009**, *15*, 6415–6427.
- (65) Smith, A. R. G.; Burn, P. L.; Powell, B. J. Spin–Orbit Coupling in Phosphorescent Iridium(III) Complexes. *ChemPhysChem* **2011**, *12*, 2429–2438.
- (66) It should be noted that, upon protonation, the luminescences of Ir-pzpy, Ir-bpz, and Ir-TAP are quenched (data not shown). This quenching is attributed to the lowering of the LUMO, enhancing radiationless deactivation according to the energy gap law.
- (67) Zanoni, K. P. S.; Kariyazaki, B. K.; Ito, A.; Brennaman, M. K.; Meyer, T. J.; Murakami Iha, N. Y. Blue-Green Iridium(III) Emitter and Comprehensive Photophysical Elucidation of Heteroleptic Cyclometalated Iridium(III) Complexes. *Inorg. Chem.* **2014**, *53*, 4089–4099.
- (68) Chen, P.; Meyer, T. J. Electron Transfer in Frozen Media. *Inorg. Chem.* **1996**, *35*, 5520–5524.
- (69) Chen, P.; Meyer, T. J. Medium Effects on Charge Transfer in Metal Complexes. *Chem. Rev.* **1998**, *98*, 1439–1478.
- (70) Brouwer, A. M. Standards for photoluminescence quantum yield measurements in solution (IUPAC Technical Report). *Pure Appl. Chem.* **2011**, *83*, 2213–2228.
- (71) Caspar, J. V.; Westmoreland, T. D.; Allen, G. H.; Bradley, P. G.; Meyer, T. J.; Woodruff, W. H. Molecular and electronic structure in the metal-to-ligand charge-transfer excited states of d₆ transition-metal complexes in solution. *J. Am. Chem. Soc.* **1984**, *106*, 3492–3500.
- (72) Allen, G. H.; White, R. P.; Rillema, D. P.; Meyer, T. J. Synthetic control of excited-state properties. Tris-chelate complexes containing the ligands 2,2'-bipyrazine, 2,2'-bipyridine, and 2,2'-bipyrimidine. *J. Am. Chem. Soc.* **1984**, *106*, 2613–2620.
- (73) Streckas, T. C.; Diamandopoulos, P. S. Surface-enhanced raman spectroscopy of bipyridines and phenylpyridines. *J. Phys. Chem.* **1990**, *94*, 1986–1991.
- (74) Natarajan, L. V.; Humphreys, L. R.; Chang, R. The Singlet Quenching of Chlorophyll b by Charge Transfer Interaction with Quinones. *Spectrosc. Lett.* **1985**, *18*, 219–227.
- (75) Balzani, V.; Bergamini, G.; Campagna, S.; Puntoriero, F. In *Photochemistry and Photophysics of Coordination Compounds I*; Balzani, V., Campagna, S., Eds.; Springer Berlin Heidelberg: Berlin, Heidelberg, 2007; pp 1–36.
- (76) Valeur, B.; Berberan-Santos, M. N. In *Molecular Fluorescence*; Wiley-VCH: Weinheim, Germany, 2012; pp 141–179.
- (77) Rehm, D.; Weller, A. Kinetics of Fluorescence Quenching by Electron and H-Atom Transfer. *Isr. J. Chem.* **1970**, *8*, 259–271.
- (78) Steenken, S.; Jovanovic, S. V. How Easily Oxidizable Is DNA? One-Electron Reduction Potentials of Adenosine and Guanosine Radicals in Aqueous Solution. *J. Am. Chem. Soc.* **1997**, *119*, 617–618.
- (79) Burrows, C. J.; Muller, J. G. Oxidative Nucleobase Modifications Leading to Strand Scission. *Chem. Rev.* **1998**, *98*, 1109–1152.